10 YEARS ANNIVERSARY

INORGANIC CHEMISTRY

FRONTIERS

RESEARCH ARTICLE

Check for updates

Soft seed-mediated dimensional control of metal–organic framework nanocrystals through oil-in-water microemulsions†

Jaedeok Lee,‡[a] Suhyeon Park,‡[a] Seojeong Woo,[a] Cheongwon Bae,[a] Yuri Jeon,[a] Mingyu Gu,[a] Jeongeon Kim,[a] Yeram Kim,[a] Sang Yong Nam, [ID][b] Jong Hwa Jung [ID][a] and Juyeong Kim [ID] *[a]

Metal–organic framework (MOF) nanocrystals with high surface area and morphological tunability have shown great potential for a wide range of industrial applications when compared with their bulk counterparts. However, achieving environment-friendly synthesis of MOF nanocrystals with minimal use of hazardous chemicals and low energy consumption remains a significant challenge. Herein, we developed a soft seed-mediated approach to synthesise nanocrystals of zeolitic imidazolate frameworks (ZIFs) in water without any assistance of chemical additives such as surfactants and organic solvents. An oil-in-water microemulsion, made from a trace amount of oil with water, was introduced to the reaction medium as the soft seed, and precise size control of ZIF-8 crystals from nanometres to micrometres was enabled by varying the volume of the oil-in-water microemulsion. Scanning electron microscopy and cryo-transmission electron microscopy analyses of the reaction intermediates revealed that the surface of the oil-in-water microemulsion functions as a nucleation site for ZIF-8 crystals, which dissipates over time. Furthermore, aromatic compounds with different numbers and lengths of alkyl chains for the oil phase were used to examine the chemical effect of the oil-in-water microemulsion on ZIF-8 crystal size, which led to fine-size control of ZIF-8 nanocrystals. Our microemulsion-induced synthesis could also be used to dimensionally control ZIF-67 crystals as well as ZIF-derived hollow nanostructures. ZIF-8 nanocrystals in our work exhibited enhanced catalytic activity for Knoevenagel condensation and dye adsorptivity with methyl orange and rhodamine B. We anticipate that our soft seed-mediated method will help improve the efficiency of MOF nanocrystal production for industrial applications.

Introduction

Metal–organic frameworks (MOFs), composed of metal ions and organic linkers in porous crystallinity, have attracted significant interest for numerous applications, including adsorption,[1–3] separation,[4–6] catalysis,[7–9] drug delivery,[10–12] and electronics[13–15], owing to their high surface area and structural tunability. Tremendous effort to produce novel microporous structures has been made by associating various organic ligands with metal ions, creating a comprehensive library of MOFs with diverse micropore size, shape and chemi-

cal affinity.[16] However, little effort has been devoted to explaining the unique features of MOFs that can be derived from differences in their nanoscale crystal size and shape, for which molecular-level structural differences may not be responsible.

Recent reports reveal that the properties of MOF crystals can have great dependency on the size[17–19] and crystal facet.[20–22] For example, when the bulk size of Fe(TA)$_2$ (TA = 1,2,3-triazolate) was reduced to 25 nm, the electronic conductivity was enhanced by ~100-fold.[23] This was because thin films of MOF nanocrystals could be densely packed in contrast to bulk crystals. Compared to that in micron-sized crystals, the gas adsorption kinetics in {[Zn(ip)(bpy)]}$_n$ (ip = isophthalate, bpy = 4,4′-bipyridyl) could be significantly enhanced with nanocrystals of a few nanometres.[24] In addition, photoinduced force microscopy showed that molecular adsorption with formaldehyde was dependent on the MOF surface facet. Gas adsorption with formaldehyde in zeolitic imidazolate framework-8 (ZIF-8) preferentially occurred at high-energy crystal facets such as edges and corners, {310} > {111} > {210} > {211}

[a]*Department of Chemistry and Research Institute of Natural Sciences, Gyeongsang National University, Jinju 52828, South Korea. E-mail: chris@gnu.ac.kr*
[b]*Department of Materials Engineering and Convergence Technology, Gyeongsang National University, Jinju 52828, South Korea*
†Electronic supplementary information (ESI) available. See DOI: https://doi.org/10.1039/d3qi01567j
‡These authors contributed equally.

> {110} ~ {100}.[25] In this regard, a comprehensive investigation of MOF characteristics in the nanoscopic regime and the establishment of a nanoscale morphology–property relationship would mitigate the current limitations in the molecular-level modulation of MOFs and facilitate the discovery of suitable MOF properties best suited for specific industrial applications.

Several synthesis strategies have been conventionally used to control the dimensions of MOFs and produce MOF nanocrystals: (i) optimising complex reaction parameters such as MOF precursors or chemical additive concentrations, solvent polarity and reaction temperature; (ii) applying intense energy with microwave or ultrasound; and (iii) limiting reaction space with microreactors.[18,26–28] Although these methods allowed dimensional engineering of MOFs, potential drawbacks to the efficiency and universality of synthesis include the time spent optimising acceptable reaction parameters, the excessive use of an energy source and the application of a substantial quantity of organic solvents. For example, chemical additives such as cetrimonium bromide (CTAB) are widely used to modify the morphology of ZIF-8 crystals.[29,30] An increase in the CTAB concentration allows their size reduction, while unavoidable shape change simultaneously occurs from a rhombic dodecahedron to a simple cube. CTAB molecules may also remain on the surface and inside a pore, requiring an additional removal process. Moreover, in contrast to the thermodynamic control provided by a hydrothermal reaction, the intense energy supply with microwaves or ultrasound could facilitate kinetic control of MOF synthesis and the formation of MOF nanocrystals in a shorter reaction time.[31–33] However, it causes excessive energy consumption and potential damage to the MOF crystal surface and structure.[34] Lastly, the confined reaction space from using a water-in-oil droplet requires surfactant molecules to stabilise the droplet as well as a large amount of organic solvent,[35,36] which may result in unwanted chemical waste.

Herein, we demonstrate an environment-friendly universal methodology to control MOF crystal dimensions from nanometres to micrometres only by introducing an oil-in-water microemulsion, totally differentiated from the conventional approaches involving excessive chemical additives, intensive energy supply and water-in-oil confined synthesis. In particular, surfactant-free oil-in-water microemulsions have not been used for MOF synthesis to the best of our knowledge, whereas water-in-oil droplets as a reverse phase were previously reported as a way to reduce MOF crystal size.[35] Using an oil-in-water microemulsion, made from a trace amount of oil with water, we produced ZIF nanocrystals with rhombic dodecahedral geometry and excellent size control. In our emulsion-mediated synthesis, the oil-in-water microemulsion was used as a nucleation site to guide ZIF formation through a heterogeneous nucleation route. Although seeded-growth synthesis is frequently used to produce metal nanocrystals with different shapes,[37,38] it is rarely adopted for MOF nanocrystals. The few examples of heterogeneous MOF nucleation and growth are limited to MOF film growth on a substrate and hybrid metal core–MOF shell structures.[39–42] Furthermore, our oil-in-water microemulsion gradually disappeared over time and was not combined with the final ZIF nanocrystals, serving as a sacrificing seed. The bulk of seeded growths with hard seed materials may not segregate the overgrown material from the seed, but our self-sacrificing seed would not interfere with the growth process of ZIFs.

In addition, using different alkyl benzene derivatives as the oil phase, we investigated the chemical effects of oil-in-water microemulsions on the dimensional control of ZIFs, enabling fine-nanoscale size modulation. We also discovered that our soft seed-mediated synthesis was applicable to ZIFs with different metal centres, ZIF-8 and ZIF-67, to further improve dimensional control when producing hollow ZIF nanostructures. Using Knoevenagel condensation with benzaldehyde and dye adsorption with methyl orange and rhodamine B, it was proved that the properties of ZIF-8 are size-dependent, with smaller ZIF-8 nanocrystals demonstrating substantial catalytic activity and adsorption capacity.

Results and discussion

An aqueous solution of zinc nitrate and 2-methylimidazole was mixed with an oil-in-water microemulsion to initiate the synthesis of ZIF-8 nanocrystals at room temperature (Fig. 1a). The oil-in-water microemulsion was prepared by vigorously agitating o-xylene and deionised water and subsequently injected into the reaction solution with ZIF-8 precursors. The volume fraction of xylene in the mixture solution was varied from 0% to 0.33% (see details in the ESI†). The addition of the microemulsion caused a significant decrease in ZIF-8 crystal size, from 2884 ± 384 nm without the microemulsion to 1600 ± 203 nm with 0.01% xylene, 272 ± 59 nm with 0.10% xylene and 166 ± 43 nm with 0.33% xylene (Fig. 1b–f and S1, ESI†). It has been generally reported that a 3 h reaction time is required to synthesise ZIF-8 in water,[40,42] while our synthesis with a 0.10% xylene microemulsion allowed much more rapid formation of ZIF-8 nanocrystals within ~5 min of stirring (Fig. S2 and S3, ESI†). The product yield after the 3 h reaction increased with higher xylene volume ratios, from 33% without the microemulsion to 34% with 0.01% xylene, 77% with 0.10% xylene and 90% with 0.33% xylene. Note that our method was optimised on a small scale, and multiple batches of the product at each condition were collected to obtain reliable yield data. After the reaction was terminated, the remaining xylene could be segregated from the milky production solution (Fig. S4, ESI†). Without the microemulsion, ZIF-8 crystals exhibited a rhombic dodecahedral shape and rough surfaces (Fig. 1b). When produced with 0.01% xylene, the crystal facets became smooth (Fig. 1c). As the volume ratio of xylene increased to 0.10%, the ZIF-8 nanocrystal restored its previous structure with defined edges and vertices (Fig. 1d). With 0.33% xylene, ZIF-8 nanocrystals of atypical rhombic dodecahedral shape were generated (Fig. 1e). Because of their thermodynamically stable rhombic dodecahedral shape with 12 {110} faces,[43] ZIF-8 nanocrystals synthesised with 0.01% and 0.33% xylene

This journal is © the Partner Organisations 2023

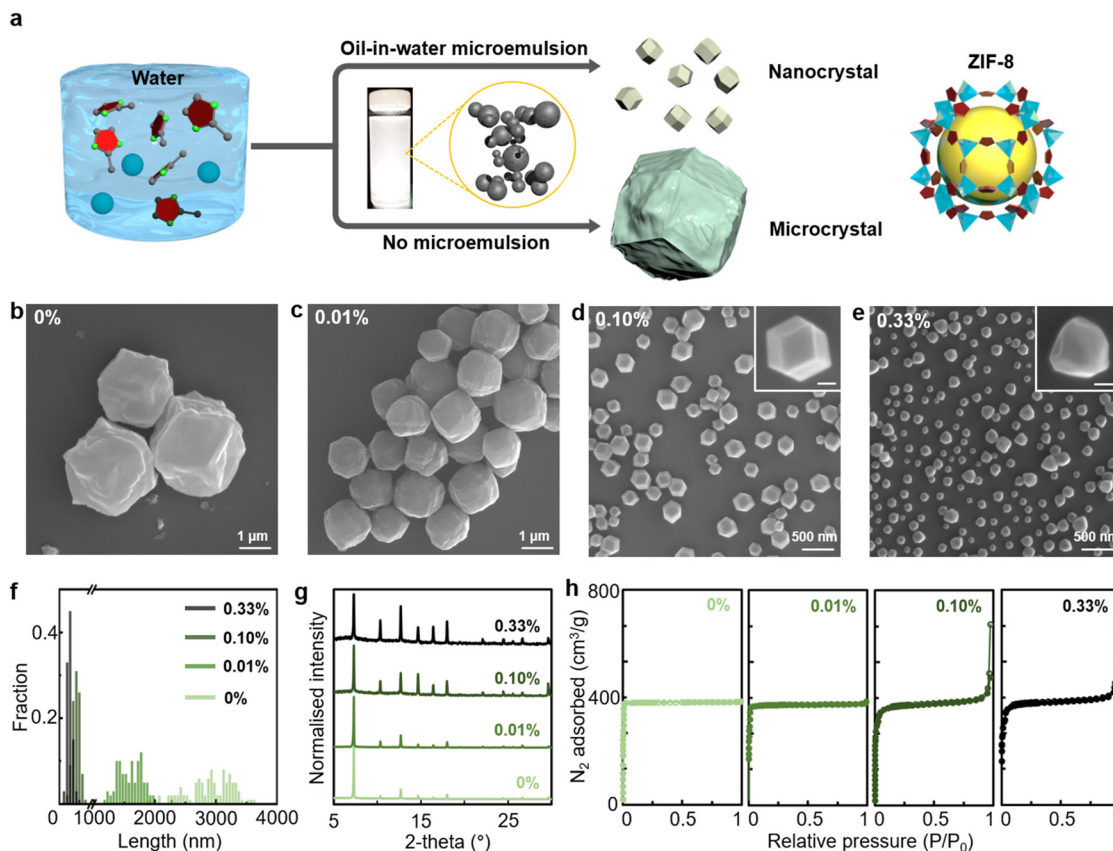*Inorg. Chem. Front.*, 2023, **10**, 7146–7154 | **7147**

Fig. 1 (a) Schematic representation of oil-in-water microemulsion-mediated ZIF-8 nanocrystal formation (pale blue sphere: Zn^{2+} ion, dark red pentagon: 2-methylimidazole, gray sphere: microemulsion and gray emerald rhombic dodecahedron: ZIF-8). (b–e) SEM images of ZIF-8 crystals generated by the addition of microemulsions with different xylene volume ratios (b: 0%, c: 0.01%, d: 0.10% and e: 0.33%). (f) Length distribution histograms for ZIF-8 crystals with different xylene volume ratios (light green: 0%, green: 0.01%, dark green: 0.10% and black: 0.33%). (g) XRD patterns of ZIF-8 crystals with different xylene volume ratios (light green: 0%, green: 0.01%, dark green: 0.10% and black: 0.33%). (h) Isothermal linear plots for N_2 adsorption and desorption with ZIF-8 crystals with different xylene volume ratios (light green: 0%, green: 0.01%, dark green: 0.10% and black: 0.33%). Scale bar: 100 nm for the inset images in (d) and (e).

could be recognised as intermediate shapes. As the micrometre-scale crystal was produced with 0.01% xylene (Fig. 1c), the thermodynamically controlled growth of ZIF-8 is regarded as dominating. Thus, a shortage of ZIF-8 precursors led to the formation of a pseudo-rhombic dodecahedral morphology, which could have further transformed into the equilibrium rhombic dodecahedral morphology. On the other hand, ZIF-8 nanocrystals with distorted morphology were generated with 0.33% xylene (Fig. 1e). As the volume of xylene increased ~3 times over that of 0.10% xylene, it was anticipated that high-density microemulsions would have greater spatial contact with ZIF-8 nanocrystals during the growth process, preventing the equilibrium crystal facet growth of the rhombic dodecahedral morphology. Furthermore, we attempted a scale-up reaction with 0.10% xylene for bulk synthesis (Fig. S5, ESI†). The scale-up was conducted with volumes of 6 mL (fourfold scale-up), 12 mL (eightfold scale-up) and 60 mL (fortyfold scale-up). The size of the ZIF-8 crystals was measured as 464 ± 105 nm for the 6 mL scale-up, 573 ± 106 nm for the 12 mL scale-up and 477 ± 127 nm for the 60 mL scale-up. In contrast to the

original scale synthesis, the particle size from the scale-up reactions was rather increased by a factor of approximately 2. The particle morphology became more irregular in shape than that of the rhombic dodecahedron. We consider that further engineering will be needed for large-scale synthesis.

Fig. 1g presents X-ray diffraction (XRD) data obtained for ZIF-8 under each condition. Despite the addition of a microemulsion during synthesis, all resultant crystals exhibited the characteristic peaks of ZIF-8 (7.3° for {011}, 10.3° for {002} and 12.7° for {011}),[44] indicating a high degree of porous crystallinity. The dried ZIF-8 crystals were pretreated under vacuum at 200 °C for 6 h before measuring the specific surface area. Using the Brunauer–Emmett–Teller method, it was observed that the specific surface area of ZIF-8 crystals increased from 1212 m^2 g^{-1} in the absence of the microemulsion to 1257 m^2 g^{-1} with 0.01% xylene, 1279 m^2 g^{-1} with 0.10% xylene and 1298 m^2 g^{-1} with 0.33% of xylene (Fig. 1h and Table S1, ESI†). This was attributed to an increase in the interparticle spacing area as ZIF nanocrystals became smaller, which led to an increase in N_2 adsorption–desorption signals at high relative

7148 | *Inorg. Chem. Front.*, 2023, **10**, 7146–7154

This journal is © the Partner Organisations 2023

pressures. The total pore volume with 0.10% xylene increased twofold compared with that without the microemulsion due to the increased interparticle spacing with smaller ZIF-8 crystals (Table S1, ESI†). In addition, thermogravimetric analysis (TGA) and elemental analysis were conducted for ZIF-8 crystals with and without 0.10% xylene (Fig. S6 and Table S2, ESI†). It appeared that there could be more guest molecules present in ZIF-8 crystals with 0.10% xylene. Their TGA curve showed a greater reduction in weight percent between 100 and 300 °C than that of those synthesised without microemulsion (Fig. S6, ESI†). Moreover, the elemental analysis displayed a greater proportion of C (54.453%) and H (6.6839%) for ZIF-8 crystals with 0.10% xylene than for those synthesised without the microemulsion (C: 40.189% and H: 4.2539%). We employ an oil-in-water microemulsion strategy as opposed to the conventional water-in-oil emulsion which is composed of surfactant-stabilised water droplets. It has been demonstrated that the water-in-oil emulsion enhances the formation of ZIF-8 nanocrystals by keeping the aqueous precursors, 2-methylimidazole and zinc nitrate inside the spatially confined water phase of the emulsion.[36] On the other hand, the oil-in-water microemulsion used in our method does not function as a spatially confined microreactor, since the ZIF-8 precursors are not dissolved in the confined oil phase. This still permits precise size control of ZIF-8 crystals.

To elucidate our oil-in-water-induced synthesis of ZIF-8 nanocrystals, we studied the physical behaviour of an oil-in-water microemulsion by optical microscopy (Fig. 2a and b) and the formation process of ZIF-8 crystals at the early stages of synthesis by scanning electron microscopy (SEM) (Fig. 2c and d). Note that a benzene-based oil-in-water microemulsion was utilised as a comparison (Fig. S7, ESI†), in which ZIF-8 crystals formed with 0.10% benzene were still as large as 2428 ± 383 nm in contrast to significant size reduction with 0.10% xylene. Although benzene is highly non-polar, its water solubility is approximately 10-fold higher than that of xylene. A benzene-based microemulsion could be formed in much smaller quantities and could be less stable than a xylene-based microemulsion. First of all, both benzene- and xylene-based microemulsion solutions exhibited macroscopically noticeable droplets that gradually dissipated over time (Fig. 2a, b and Movies S1, S2, ESI†). Xylene-based microemulsion solutions disperse light more than benzene-based solutions, indicating a higher density of microemulsion droplets in the solution. The optical micrographs validate the conclusion that the benzene-based microemulsion solution presented few emulsion droplets, whereas the xylene-based solution contained numerous emulsion droplets. In addition, xylene-based microemulsion solutions with different xylene volume ratios from 0.10 to 3.33% displayed more droplet scattering with higher xylene ratios, while immediate coalescence of the microemulsions was seen with a ratio of 3.33%, the highest xylene ratio (Movie S3, ESI†). Excessive density of xylene-based microemulsions led to the rapid fusion of emulsion; thus, the higher xylene ratios over 1.00% were not effective in our ZIF-8 nanocrystal formation.
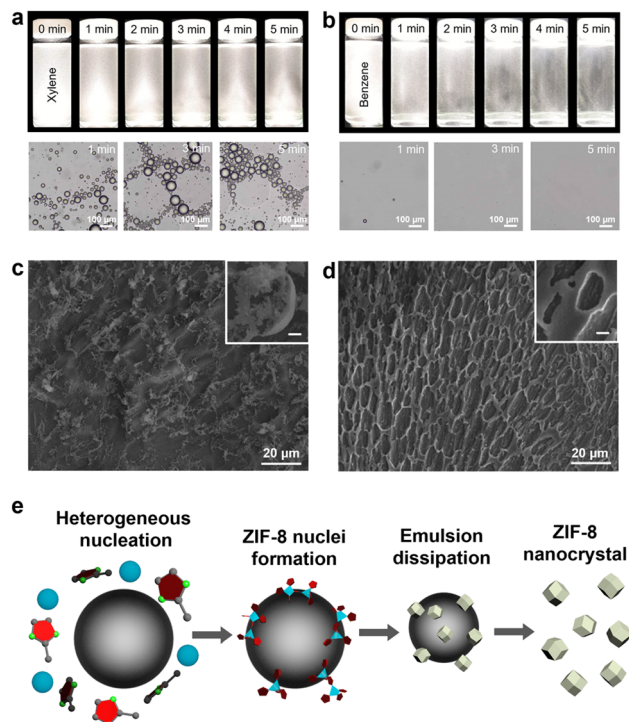

Fig. 2 Time-lapse photographs (top) and optical microscopy images (bottom) of (a) the 0.10% xylene-based microemulsion and (b) the 0.10% benzene-based microemulsion. *Ex situ* SEM images of ZIF-8 crystals captured at 3 min of reaction by (c) the 0.10% xylene-based microemulsion and (d) the 0.10% benzene-based microemulsion. (e) Schematics of microemulsion-mediated nucleation and growth of ZIF-8 crystals (pale blue sphere: Zn^{2+} ion, dark red pentagon: 2-methylimidazole, gray sphere: microemulsion and gray emerald rhombic dodecahedron: ZIF-8). Scale bar: 1 μm for the inset images in (c) and (d).

We further studied the influence of microemulsion density on ZIF-8 crystal growth from 1 to 5 min of reaction using SEM (Fig. 2c, d and S8, ESI†). To preserve the pristine state of the samples, an aliquot (10 μL) was collected every minute from the reaction solution and placed on a Si wafer. Then, it was rapidly dried under vacuum. We examined the macroscopic arrangement of ZIF-8 crystal intermediates to figure out microemulsion-involved changes on ZIF-8 formation. Deposition patterns of early-stage ZIF-8 intermediates up to 2 min were similar to each other with both xylene-based and benzene-based microemulsions used. However, after 3 min of reaction, distinct changes in the macroscopic arrangement of ZIF-8 intermediates were observed as aggregates preserving a hemispherical shape with xylene-based microemulsions (Fig. 2c) in contrast to flat aggregate deposition with benzene-based microemulsions (Fig. 2d). As ZIF-8 crystal growth progressed, such curved patterns were clearly recognised throughout a large region with xylene-based microemulsions (Fig. S8, ESI†). Moreover, using cryogenic transmission electron microscopy (cryo-TEM), we investigated the reaction solution with 0.10% xylene-based microemulsions frozen at a very early stage (see specimen preparation in the ESI†). The cryo-TEM images

This journal is © the Partner Organisations 2023

Inorg. Chem. Front., 2023, **10**, 7146–7154 | **7149**

showed that small particles were present around a micro-emulsion droplet (Fig. S9, ESI†). We supposed that the aggregates were most likely ZIF-8 intermediates formed *via* rapid nucleation at the microemulsion interfaces.

Based on our electron microscopy analyses, we could suggest the formation mechanism for ZIF-8 nanocrystals induced by the oil-in-water microemulsion (Fig. 2e). ZIF-8 crystal nucleation could occur preferentially in the vicinity of xylene-based microemulsions, which would explain why most of the ZIF-8 intermediates appeared as though enclosing a spherical object. This was attributed the oil-in-water micro-emulsion being able to accelerate the formation of ZIF-8 nuclei by reducing the surface tension of the reaction medium at the interface of the microemulsion droplet.[45] At the same time, an increase in the concentration of 2-methylimidazolate could occur at the oil/water interface (Fig. S10, ESI†). Although 2-methylimidazolate after being deprotonated is hardly soluble in xylene due to the large difference in polarity, it may be attracted to the surface of the microemulsion because of its aromatic ring that can have van der Waals attraction with xylene of the microemulsion.[46] Locally concentrated ligands near the microemulsion would promote the formation of ZIF-8 nuclei compared to the bulk solution.[47] In recent studies, the manipulation of nucleation processes of MOF crystals by increasing the initial reactant concentrations helped control the size of MOF crystals.[48] However, excessive reactant concentrations can hinder the crystal growth and crystallisation of MOFs during the reaction.[49] In our investigation, the micro-emulsion accelerated the nucleation process of ZIF-8 crystals, resulting in rapid reactant consumption as well as shortened growth. As the ZIF-8 growth proceeds, the microemulsion gradually dissipates, resulting in only ZIF-8 nanocrystals. In this regard, our oil-in-water microemulsion serves as a sacrifice seed whose primary aim is to promote the nucleation of ZIF-8. This soft seed-mediated approach is differentiated from conventional seeded-growth methods, where the seeds are generally incorporated in the final structure such as seed-grown anisotropic gold nanoparticles[37] and MOF-on-MOF hybrid structures.[50] Note that dissolution of xylene from the oil-in-water microemulsion into water would not disrupt our suggested formation mechanism because of its poor water solubility.[51] Also, we excluded any possibility that the ZIF-8 precursors were partially dissolved in the oil phase, since the large majority of the precursors were dissolved in the water phase due to their high water solubility.

To investigate the chemical effects of the oil phase in the oil-in-water microemulsion on the number and length of alkyl chains, a variety of aromatic derivatives were used (Fig. 3). A microemulsion containing several aromatic derivatives, respectively, enabled precise control over the size of ZIF-8 crystals. To determine the effect of the number of methyl groups, benzene, toluene and xylene were utilised at 0.10%. The crystal size of ZIF-8 was determined as 2428 ± 383 nm with benzene, 352 ± 117 nm with toluene and 272 ± 59 nm with xylene (Fig. 3a and S11, ESI†). As previously stated, benzene-based microemulsions in water had a significantly lower density than
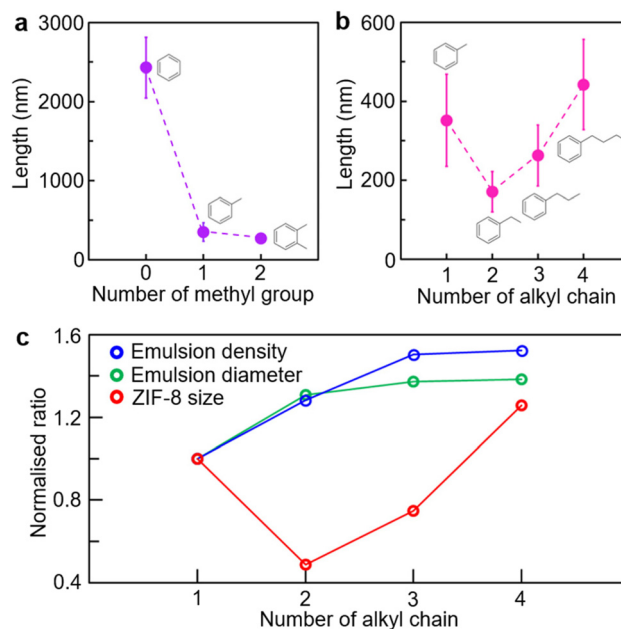

Fig. 3 (a) ZIF-8 crystal size as a function of the number methyl groups on the aromatic ring (0: benzene, 1: toluene and 2: xylene). (b) ZIF-8 crystal size as a function of alkyl chain length on the aromatic ring (1: toluene, 2: ethylbenzene, 3: propylbenzene and 4: butylbenzene). (c) Normalised ratio values of microemulsion density (blue circle), micro-emulsion diameter (green circle) and ZIF-8 crystal size (red circle) as a function of alkyl chain length on the aromatic ring. The ratio values were normalised with respect to each measurement with the toluene-based microemulsion. The dotted and solid lines in (a–c) serve as visual aids.

xylene-based microemulsions, and they had negligible effects on the reduction of ZIF-8 crystal size. The toluene-based micro-emulsion could produce ZIF-8 nanocrystals, although the xylene-based microemulsion was the most effective in terms of size reduction. Additionally, 0.10% ethylbenzene, *n*-propylbenzene and *n*-butylbenzene were used to examine the effect of alkyl group length on the size of ZIF-8 crystals (Fig. 3b and S12, ESI†). The ethylbenzene-based microemulsion generated the smallest ZIF-8 nanocrystal (171 ± 51 nm), followed by those based on propylbenzene (262 ± 77 nm) and butylbenzene (442 ± 114 nm). The profile of alkyl chain length as a function of ZIF-8 crystal size exhibited the shape of a valley when the toluene-based microemulsion was added.

Analyses of the microemulsion diameter (X_{90}) and density estimated from dynamic light scattering (DLS) highlight the relationship between the two variables for ZIF-8 size control (Fig. 3c). Note that the microemulsion density was estimated based on the count rate measured by DLS, since the same volume of the microemulsion solution was used for each measurement. The diameter and density of the microemulsion increased with increasing chain length (Fig. S13, ESI†). The toluene-based microemulsion had a diameter of 370 ± 18 nm, while ethylbenzene had a 484 ± 69 nm diameter, propylbenzene had a 508 ± 52 nm diameter and butylbenzene had a 512 ± 29 nm diameter. The mean count rate for microemulsion

7150 | *Inorg. Chem. Front.*, 2023, **10**, 7146–7154

This journal is © the Partner Organisations 2023

density was 41.7 ± 0.5 kcps for toluene, whereas that for ethyl-benzene was 53.4 ± 1.7 kcps, that for propylbenzene was 62.7 ± 1.1 kcps and that for butylbenzene was 63.5 ± 2.3 kcps. Such correlation between microemulsion diameter and density and ZIF-8 dimensions could correspond to the xylene volume effect (Fig. S13, ESI†), in that the number of nucleation sites for ZIF-8 crystals increased as the interfacial area of micro-emulsions increased. However, ZIF-8 nanocrystals began to grow larger from propylbenzene in spite of the increasing microemulsion diameter and density. We assume that the chemical effect predominated in propylbenzene-based micro-emulsions due to the increased hydrophobicity of the long alkyl chain, which could hinder 2-methylimidazolate from being locally concentrated at the microemulsion surface and prevent ZIF-8 nucleation on the microemulsion surface.

We applied our method to ZIF-67 which is composed of a cobalt metal centre (Fig. 4a–d). The microemulsion-mediated process was suitable for controlling the size of ZIF-67 crystals. As the volume of xylene was increased in the microemulsion solution, there was a significant size reduction of ZIF-67 crys-

Fig. 5 (a) Conversion rate for the Knoevenagel condensation reaction of malononitrile with benzaldehyde as a function of time using ZIF-8 nanocrystals generated by the 0.10% xylene-based microemulsion (dark green circle), ZIF-8 microcrystals (light green circle) and no catalyst. (b) Adsorption of methyl orange (left bar graph set) and rhodamine B (right bar graph set). The dark green bars correspond to dye adsorptivity by ZIF-8 nanocrystals generated by the 0.10% xylene-based microemulsion and the light green bars correspond to dye adsorptivity by ZIF-8 microcrystals.

tals from 2168 ± 609 nm with 0% to 1264 ± 120 nm with 0.03% and 827 ± 97 nm with 0.10% (Fig. S14 and S15, ESI†). In addition, the facile size control of ZIF-67 crystals was essential for the development of hollow nanostructures of different sizes (Fig. 4e and f). The hollow nanostructure was synthesised using the size-controlled ZIF-67 nanocrystals as a template, followed by coating ZIF-8 adlayers on the ZIF-67 surface and subsequently etching ZIF-67 from the core (see details in the ESI†).

The catalytic potential and dye-adsorption potential of emulsion-induced ZIF-8 nanocrystals were studied with respect to their size reduction effect and increased surface area (Fig. 5). The heterogeneous catalytic activity of ZIF-8 nanocrystals produced from a 0.10% xylene-based microemulsion was evaluated for the Knoevenagel condensation of malononitrile and benzaldehyde as shown in Fig. 5a and S16, ESI.† Micron-sized ZIF-8 particles generated without a microemulsion were used for comparison purposes. The conversion rate of ZIF-8 nanocrystals with 0.10% xylene was higher than that of micron-sized ZIF-8 particles, 46.6% after 30 min, 62.1% after 1 h, 72.0% after 2 h, 87.7% after 4 h and 93.4% after 6 h. The greater conversion rate was attributed to the higher external surface area of the smaller ZIF-8 nanocrystals produced by the 0.10% xylene-based microemulsion (Table S3, ESI†). Additionally, the ability of the two types of ZIF-8 crystals to adsorb methyl orange and rhodamine B was investigated and is presented in Fig. 5b and S17–S20, ESI.† ZIF-8 nanocrystals produced by the 0.10% xylene-based microemulsion exhibited ~5-fold enhanced adsorptivity (4.8 mg g^{-1}) for methyl orange in comparison with the micron-sized ZIF-8 particles (0.9 mg g^{-1}) (Table S4, ESI†). There was also an ~7-fold enhancement in the adsorption of rhodamine B: 1.4 mg g^{-1} by the micron-sized ZIF-8 particles and 10.0 mg g^{-1} by ZIF-8 nanocrystals produced by the 0.10% xylene-based microemulsion (Table S5, ESI†).
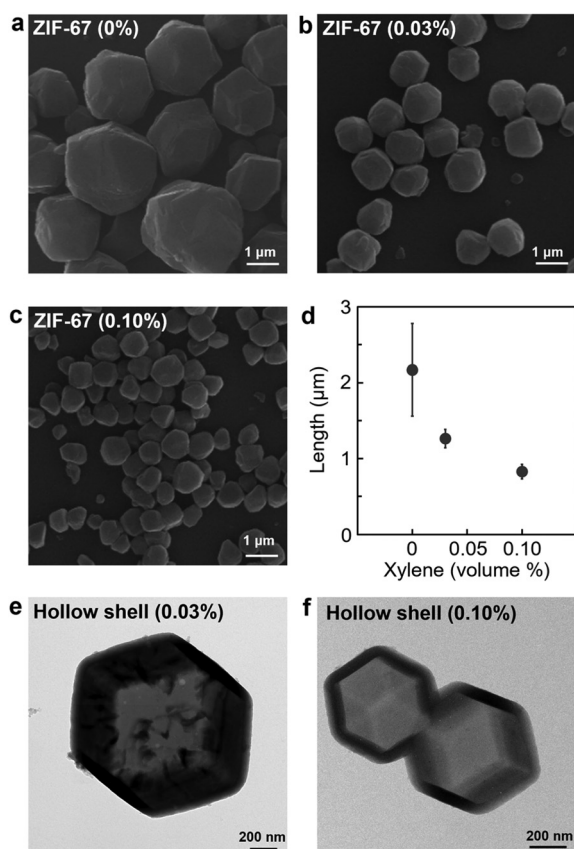

Fig. 4 (a–c) SEM images of ZIF-67 crystals generated by the addition of microemulsion with different volume ratios of xylene (a: 0%, b: 0.03% and c: 0.10%). (d) ZIF-67 crystal size as a function of xylene volume (left: 0%, middle: 0.03% and right: 0.10%). TEM images of hollow nano-structures made from ZIF-67 crystals produced using (e) the 0.03% xylene-based microemulsion and (f) the 0.10% xylene-based microemulsion.
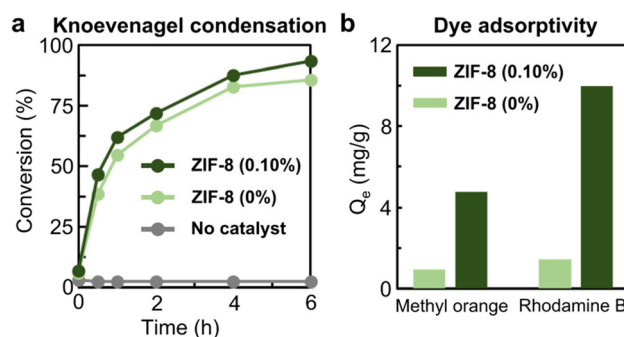
This journal is © the Partner Organisations 2023

Inorg. Chem. Front., 2023, **10**, 7146–7154 | **7151**

Conclusions

We demonstrated that through the use of an oil-in-water microemulsion, soft seeds can exert dimensional control over ZIFs. With a greater volume ratio of xylene to water, the oil-in-water microemulsion produced ZIF nanocrystals with a uniform size and shape. *Ex situ* SEM and cryo-TEM analyses of time-dependent formation processes revealed that oil-in-water microemulsions could serve as ZIF-8 nucleation sites and be self-sacrificed during the reaction rather than being incorporated. Furthermore, we discovered that the particle size could be altered by using a range of aromatic compounds as the oil phase in the microemulsion. In terms of the microemulsion diameter and density, shorter chains were susceptible to physical interactions, whereas longer chains were dominated by chemical effects. The use of the oil-in-water microemulsion as a seed could also be applicable to ZIF-67, allowing for size reduction relative to the volume of the oil phase and promoting advanced topologies such as hollow morphology. Compared to micron-sized ZIF-8 particles, the nanoscopic crystals produced with the microemulsion exhibited enhanced catalytic activity for the Knoevenagel condensation reaction and enhanced dye adsorption with methyl orange and rhodamine B. Our methodology with the soft seed-mediated dimensional control of MOFs using oil-in-water microemulsions would be more sustainable and applicable in industrial fields than conventional techniques for synthesising MOF nanocrystals.

Author contributions

Conceptualisation, J. L. and J. K.; validation, J. L. and S. P.; formal analysis, J. L., S. P., S. W., C. B., Y. J., M. G., J. K. and Y. K.; writing - original draft preparation, J. L., S. P. and J. K.; writing - review and editing, J. L., S. P., S. W., C. B., M. G., S. Y. N., J. H. J., and J. K.; visualisation, J. L., S. P. and C. B.; supervision, J. K.; project administration, S. Y. N., J. H. J., and J. K.; and funding acquisition, S. Y. N., J. H. J. and J. K.

Conflicts of interest

There are no conflicts to declare.

Acknowledgements

References

1 J.-R. Li, R. J. Kuppler and H.-C. Zhou, Selective gas adsorption and separation in metal–organic frameworks, *Chem. Soc. Rev.*, 2009, **38**, 1477–1504.

2 N. C. Burtch, H. Jasuja and K. S. Walton, Water stability and adsorption in metal–organic frameworks, *Chem. Rev.*, 2014, **114**, 10575–10612.

3 C. Bae, M. Gu, Y. Jeon, D. Kim and J. Kim, Metal–organic frameworks for NH_3 adsorption by different NH_3 operating pressures, *Bull. Korean Chem. Soc.*, 2023, **44**, 112–124.

4 B. Liu, Metal–organic framework-based devices: Separation and sensors, *J. Mater. Chem.*, 2012, **22**, 10094–10101.

5 M. S. Denny, J. C. Moreton, L. Benz and S. M. Cohen, Metal–organic frameworks for membrane-based separations, *Nat. Rev. Mater.*, 2016, **1**, 16078.

6 X. Zhao, Y. Wang, D.-S. Li, X. Bu and P. Feng, Metal–organic frameworks for separation, *Adv. Mater.*, 2018, **30**, 1705189.

7 J. Lee, O. K. Farha, J. Roberts, K. A. Scheidt, S. T. Nguyen and J. T. Hupp, Metal–organic framework materials as catalysts, *Chem. Soc. Rev.*, 2009, **38**, 1450–1459.

8 J. Liu, L. Chen, H. Cui, J. Zhang, L. Zhang and C.-Y. Su, Applications of metal–organic frameworks in heterogeneous supramolecular catalysis, *Chem. Soc. Rev.*, 2014, **43**, 6011–6061.

9 D. Yang and B. C. Gates, Catalysis by metal organic frameworks: perspective and suggestions for future research, *ACS Catal.*, 2019, **9**, 1779–1798.

10 P. Horcajada, T. Chalati, C. Serre, B. Gillet, C. Sebrie, T. Baati, J. F. Eubank, D. Heurtaux, P. Clayette, C. Kreuz, J.-S. Chang, Y. K. Hwang, V. Marsaud, P.-N. Bories, L. Cynober, S. Gil, G. Férey, P. Couvreur and R. Gref, Porous metal–organic-framework nanoscale carriers as a potential platform for drug delivery and imaging, *Nat. Mater.*, 2010, **9**, 172–178.

11 M.-X. Wu and Y.-W. Yang, Metal–organic framework (MOF)-based drug/cargo delivery and cancer therapy, *Adv. Mater.*, 2017, **29**, 1606134.

12 H. D. Lawson, S. P. Walton and C. Chan, Metal–organic frameworks for drug delivery: A design perspective, *ACS Appl. Mater. Interfaces*, 2021, **13**, 7004–7020.

13 A. A. Talin, A. Centrone, A. C. Ford, M. E. Foster, V. Stavila, P. Haney, R. A. Kinney, V. Szalai, F. El Gabaly, H. P. Yoon, F. Léonard and M. D. Allendorf, Tunable electrical conductivity in metal–organic framework thin-film devices, *Science*, 2014, **343**, 66–69.

14 J. Wu, J. Chen, C. Wang, Y. Zhou, K. Ba, H. Xu, W. Bao, X. Xu, A. Carlsson, S. Lazar, A. Meingast, Z. Sun and H. Deng, Metal–organic framework for transparent electronics, *Adv. Sci.*, 2020, **7**, 1903003.

7152 | *Inorg. Chem. Front.*, 2023, **10**, 7146–7154

This journal is © the Partner Organisations 2023

15 V. Aggarwal, S. Solanki and B. D. Malhotra, Applications of metal–organic framework-based bioelectrodes, *Chem. Sci.*, 2022, **13**, 8727–8743.

16 H. Furukawa, K. E. Cordova, M. O'Keeffe and O. M. Yaghi, The chemistry and applications of metal–organic frameworks, *Science*, 2013, **341**, 1230444.

17 S. Wang, C. M. McGuirk, A. d'Aquino, J. A. Mason and C. A. Mirkin, Metal–organic framework nanoparticles, *Adv. Mater.*, 2018, **30**, 1800202.

18 C. R. Marshall, S. A. Staudhammer and C. K. Brozek, Size control over metal–organic framework porous nanocrystals, *Chem. Sci.*, 2019, **10**, 9396–9408.

19 K. Fabrizio and C. K. Brozek, Size-dependent thermal shifts to MOF nanocrystal optical gaps induced by dynamic bonding, *Nano Lett.*, 2023, **23**, 925–930.

20 F. Guo, J.-H. Guo, P. Wang, Y.-S. Kang, Y. Liu, J. Zhao and W.-Y. Sun, Facet-dependent photocatalytic hydrogen production of metal–organic framework NH_2-MIL-125(Ti), *Chem. Sci.*, 2019, **10**, 4834–4838.

21 W. Yang, H.-J. Wang, R.-R. Liu, J.-W. Wang, C. Zhang, C. Li, D.-C. Zhong and T.-B. Lu, Tailoring crystal facets of metal–organic layers to enhance photocatalytic activity for CO_2 reduction, *Angew. Chem., Int. Ed.*, 2021, **60**, 409–414.

22 X.-Y. Zhang, P. Wang, Y. Zhang, X.-M. Cheng and W.-Y. Sun, Facet-dependent photocatalytic behavior of Fe-Soc-MOF for carbon dioxide reduction, *ACS Appl. Mater. Interfaces*, 2023, **15**, 3348–3356.

23 C. R. Marshall, J. P. Dvorak, L. P. Twight, L. Chen, K. Kadota, A. B. Andreeva, A. E. Overland, T. Ericson, A. F. Cozzolino and C. K. Brozek, Size-dependent properties of solution-processable conductive MOF nanocrystals, *J. Am. Chem. Soc.*, 2022, **144**, 5784–5794.

24 D. Tanaka, A. Henke, K. Albrecht, M. Moeller, K. Nakagawa, S. Kitagawa and J. Groll, Rapid preparation of flexible porous coordination polymer nanocrystals with accelerated guest adsorption kinetics, *Nat. Chem.*, 2010, **2**, 410–416.

25 G. Delen, M. Monai, K. Stančiaková, B. Baumgartner, F. Meirer and B. M. Weckhuysen, Structure sensitivity in gas sorption and conversion on metal–organic frameworks, *Nat. Commun.*, 2023, **14**, 129.

26 N. Stock and S. Biswas, Synthesis of metal–organic frameworks (MOFs): Routes to various MOF topologies, morphologies, and composites, *Chem. Rev.*, 2012, **112**, 933–969.

27 N. A. Khan and S. H. Jhung, Synthesis of metal–organic frameworks (MOFs) with microwave or ultrasound: Rapid reaction, phase-selectivity, and size reduction, *Coord. Chem. Rev.*, 2015, **285**, 11–23.

28 J. Troyano, A. Carné-Sánchez, C. Avci, I. Imaz and D. Maspoch, Colloidal metal–organic framework particles: The pioneering case of ZIF-8, *Chem. Soc. Rev.*, 2019, **48**, 5534–5546.

29 Y. Pan, D. Heryadi, F. Zhou, L. Zhao, G. Lestari, H. Su and Z. Lai, Tuning the crystal morphology and size of zeolitic imidazolate framework-8 in aqueous solution by surfactants, *CrystEngComm*, 2011, **13**, 6937–6940.

30 G. Zheng, Z. Chen, K. Sentosun, I. Pérez-Juste, S. Bals, L. M. Liz-Marzán, I. Pastoriza-Santos, J. Pérez-Juste and M. Hong, Shape control in ZIF-8 nanocrystals and metal nanoparticles@ZIF-8 heterostructures, *Nanoscale*, 2017, **9**, 16645–16651.

31 S. H. Jhung, J.-H. Lee, J. W. Yoon, C. Serre, G. Férey and J.-S. Chang, Microwave synthesis of chromium terephthalate MIL-101 and its benzene sorption ability, *Adv. Mater.*, 2007, **19**, 121–124.

32 E. Haque and S. H. Jhung, Synthesis of isostructural metal–organic frameworks, CPO-27s, with ultrasound, microwave, and conventional heating: Effect of synthesis methods and metal ions, *Chem. Eng. J.*, 2011, **173**, 866–872.

33 W. Liang and D. M. D'Alessandro, Microwave-assisted solvothermal synthesis of zirconium oxide based metal–organic frameworks, *Chem. Commun.*, 2013, **49**, 3706–3708.

34 S. Nalesso, G. Varlet, M. J. Bussemaker, R. P. Sear, M. Hodnett, R. Monteagudo-Oliván, V. Sebastián, J. Coronas and J. Lee, Sonocrystallisation of ZIF-8 in water with high excess of ligand: Effects of frequency, power and sonication time, *Ultrason. Sonochem.*, 2021, **76**, 105616.

35 W. Sun, X. Zhai and L. Zhao, Synthesis of ZIF-8 and ZIF-67 nanocrystals with well-controllable size distribution through reverse microemulsions, *Chem. Eng. J.*, 2016, **289**, 59–64.

36 R. Tatewaki, T. Yamaki, M. Yoshimune, H. Negishi, T. Imura, H. Sakai and N. Hara, Control of ZIF-7-III aspect ratio using water-in-oil microemulsion, *Colloids Surf., A*, 2020, **603**, 125157.

37 A. R. Tao, S. Habas and P. Yang, Shape control of colloidal metal nanocrystals, *Small*, 2008, **4**, 310–325.

38 S. G. Kwon, G. Krylova, P. J. Phillips, R. F. Klie, S. Chattopadhyay, T. Shibata, E. E. Bunel, Y. Liu, V. B. Prakapenka, B. Lee and E. V. Shevchenko, Heterogeneous nucleation and shape transformation of multicomponent metallic nanostructures, *Nat. Mater.*, 2015, **14**, 215–223.

39 M. Li and M. Dincă, Selective formation of biphasic thin films of metal–organic frameworks by potential-controlled cathodic electrodeposition, *Chem. Sci.*, 2014, **5**, 107–111.

40 G. Zheng, S. De Marchi, V. López-Puente, K. Sentosun, L. Polavarapu, I. Pérez-Juste, E. H. Hill, S. Bals, L. M. Liz-Marzán, I. Pastoriza-Santos and J. Pérez-Juste, Encapsulation of single plasmonic nanoparticles within ZIF-8 and SERS analysis of the MOF flexibility, *Small*, 2016, **12**, 3935–3943.

41 Z.-G. Gu and J. Zhang, Epitaxial growth and applications of oriented metal–organic framework thin films, *Coord. Chem. Rev.*, 2019, **378**, 513–532.

42 C. Bae, J. Lee, L. Yao, S. Park, Y. Lee, J. Lee, Q. Chen and J. Kim, Mechanistic insight into gold nanorod transformation in nanoscale confinement of ZIF-8, *Nano Res.*, 2021, **14**, 66–73.

43 J. Cravillon, C. A. Schröder, H. Bux, A. Rothkirch, J. Caro and M. Wiebcke, Formate modulated solvothermal synthesis of ZIF-8 investigated using time-resolved in situ

This journal is © the Partner Organisations 2023

Inorg. Chem. Front., 2023, **10**, 7146–7154 | **7153**

X-ray diffraction and scanning electron microscopy, *CrystEngComm*, 2012, **14**, 492–498.

44 Y. Pan, Y. Liu, G. Zeng, L. Zhao and Z. Lai, Rapid synthesis of zeolitic imidazolate framework-8 (ZIF-8) nanocrystals in an aqueous system, *Chem. Commun.*, 2011, **47**, 2071–2073.

45 S. Karthika, T. K. Radhakrishnan and P. Kalaichelvi, A review of classical and nonclassical nucleation theories, *Cryst. Growth Des.*, 2016, **16**, 6663–6681.

46 L. Henneberger and K.-U. Goss, Environmental sorption behavior of ionic and ionizable organic chemicals, *Rev. Environ. Contam. Toxicol.*, 2019, **253**, 43–64.

47 X. Liu, S. W. Chee, S. Raj, M. Sawczyk, P. Král and U. Mirsaidov, Three-step nucleation of metal–organic framework nanocrystals, *Proc. Natl. Acad. Sci. U. S. A.*, 2021, **118**, e2008880118.

48 J. Wang, J. Liu, Y. Song, S. Geng, Z. Peng, J. Yu, F. Liu, Y. Wang, S. Xi, Z. Zhang and Z. Fan, Simultaneous defect and size control of metal–organic framework nanostructures for highly efficient carbon dioxide electroreduction to multicarbon products, *ACS Mater. Lett.*, 2023, **5**, 2121–2130.

49 H. H.-M. Yeung, A. F. Sapnik, F. Massingberd-Mundy, M. W. Gaultois, Y. Wu, D. A. X. Fraser, S. Henke, R. Pallach, N. Heidenreich, O. V. Magdysyuk, N. T. Vo and A. L. Goodwin, Control of metal–organic framework crystallization by metastable intermediate pre-equilibrium species, *Angew. Chem., Int. Ed.*, 2019, **58**, 566–571.

50 D. H. Hong, H. S. Shim, J. Ha and H. R. Moon, MOF-on-MOF architectures: Applications in separation, catalysis, and sensing, *Bull. Korean Chem. Soc.*, 2021, **42**, 956–969.

51 I. Sanemasa, M. Araki, T. Deguchi and H. Nagai, Solubility measurements of benzene and the alkylbenzenes in water by making use of solute vapor, *Bull. Chem. Soc. Jpn.*, 1982, **55**, 1054–1062.

7154 | *Inorg. Chem. Front.*, 2023, **10**, 7146–7154

This journal is © the Partner Organisations 2023